Biomaterials Science

Prussian blue nanoparticles-based antigenicity and adjuvanticity trigger robust antitumor immune responses against neuroblastoma

Journal:	*Biomaterials Science*
Manuscript ID	BM-ART-12-2018-001553.R1
Article Type:	Paper
Date Submitted by the Author:	23-Jan-2019
Complete List of Authors:	Cano-Mejia, Juliana; George Washington University; University of Maryland Bookstaver, Michelle; University of Maryland Sweeney, Elizabeth; George Washington University Jewell, Christopher; University of Maryland at College Park, Fischell Department of Bioengineering Fernandes, Rohan; George Washington University, Medicine and GW Cancer Center

Journal Name

ARTICLE

Prussian blue nanoparticles-based antigenicity and adjuvanticity trigger robust antitumor immune responses against neuroblastoma

Received 00th January 20xx,
Accepted 00th January 20xx

DOI: 10.1039/x0xx00000x

www.rsc.org/

Juliana Cano-Mejia,[a,b] Michelle L. Bookstaver,[b] Elizabeth E. Sweeney,[a] Christopher M. Jewell[b,c,d,e,f] and Rohan Fernandes*[a,g]

We describe the synthesis of CpG oligodeoxynucleotide-coated Prussian blue nanoparticles (CpG-PBNPs) that function as a nanoimmunotherapy for neuroblastoma, a common childhood cancer. These CpG-PBNPs increase the antigenicity and adjuvanticity of treated tumors, ultimately driving robust antitumor immunity through a multi-pronged mechanism. CpG-PBNPs are synthesized using a facile layer-by-layer coating scheme resulting in nanoparticles that exhibit monodisperse size distributions and multiday stability without cytotoxicity. The strong, instrinsic absorption of PBNPs in the CpG-PBNPs enables ablative photothermal therapy (CpG-PBNP-PTT) that triggers tumor cell death, as well as release of tumor antigens to increase antigenicity. Simultaneously, the CpG coating functions as an exogenous molecular adjuvant that complements the endogenous adjuvants released by the CpG-PBNP-PTT (e.g. ATP, calreticulin, and HMGB1). In cell culture, coating NPs with CpG increases immunogenicity while maintaining the photothermal activity of PBNPs. When administered in a syngeneic, Neuro2a-based, murine model of neuroblastoma, CpG-PBNP-PTT results in complete tumor regression in a significantly higher proportion (70% at 60 days) of treated animals relative to controls. Further, the long-term surviving, CpG-PBNP-PTT-treated animals reject Neuro2a rechallenge, suggesting this therapy generates immunological memory. Our findings point to the importance of simultaneous cytotoxicity, antigenicity, and adjuvanticity to generate robust and persistent antitumor immune responses against neuroblastoma.

Introduction

Nanoparticle-based photothermal therapy (PTT) is a method for tumor control wherein biocompatible or bioinert nanoparticles convert incident light into heat, typically a cytotoxic thermal dose, in a process known as photothermal conversion.[1-3] Since PTT requires the convergence of nanoparticles and incident light at a specified location within the body, it is inherently a localized tumor treatment. Of emerging interest in this field is the effects of PTT on the immune system.[4-9] This is because generating a favorable antitumor immune response by PTT has the potential to effect robust and persistent treatment outcomes that are not only limited to localized treatment sites, but can extend to more distant sites of tumor dissemination.[4, 6] Therefore an emerging objective of PTT should include maximizing this "abscopal effect," whereby locally administered PTT causes shrinkage of non-treated, disseminated tumors, in addition to tumors directly in the treatment zone.[10, 11] A step toward achieving this goal is to ensure that PTT-treated tumors are undergoing immunogenic cell death (ICD) – a cell death mechanism that engages the immune system.[12] Immunogenicity of cell death is marked by release of antigens (antigenicity) and endogenous adjuvants (adjuvanticity) - such as damage-associated molecular patterns (DAMPs) - by dying tumor cells; these cues are important for eliciting a potent antitumor immune response.[12-16]

In this study, we describe Prussian blue nanoparticles (PBNPs) coated with a molecular adjuvant, CpG oligodeoxynucleotides (CpG-PBNPs) as a nanoimmunotherapy to increase the antigenicity and adjuvanticity of treated tumors. We utilize the PBNPs in CpG-PBNPs for PTT of tumors leveraging their inherent absorption in the near infrared (NIR) spectrum.[17, 18] PBNP-PTT not only elicits tumor cell death but increases antigenicity by releasing antigens from dying tumor cells.[19] The CpG oligodeoxynucleotides coated on the CpG-PBNPs are toll-like receptor 9 agonists that function as

[a] The George Washington Cancer Center, The George Washington University, Washington, DC 20052, USA.
[b] Fischell Department of Bioengineering, University of Maryland, College Park, MD 20742, USA.
[c] Robert E. Fischell Institute for Biomedical Devices, University of Maryland, College Park, MD 20742, USA.
[d] United States Department of Veterans Affairs, Maryland VA Health Care System Baltimore, MD 21201, USA.
[e] Department of Microbiology and Immunology, University of Maryland Medical School, Baltimore, MD 21205, USA.
[f] Marlene and Stewart Greenebaum Cancer Center, Baltimore, MD 21201, USA.
[g] Department of Medicine, The George Washington University, Washington, DC 20052, USA. *E-mail: rfernandes@gwu.edu, Tel: +1-202-994-0899.
Electronic Supplementary Information (ESI) available: Supplementary Figures S1-S4. See DOI: 10.1039/x0xx00000x

adjuvants to enhance the CpG-PBNPs-based nanoimmunotherapy.[20-23] We hypothesized that the increased antigenicity and adjuvanticity elicited by the CpG-PBNP-PTT would generate a robust antitumor immune response resulting in long-term tumor regression and protection against tumor rechallenge (Figure 1).

We tested this hypothesis in an immunocompetent (syngeneic) Neuro2a model of neuroblastoma.[24-26] Neuroblastoma is a common pediatric solid tumor accounting for around 15% of cancer-related deaths in children.[27, 28] Patients with high-risk neuroblastoma respond poorly to conventional therapies and overall survival for these patients has remained dismal, ranging between 40 and 50%.[29] This is because high-risk neuroblastoma is heterogeneous,[30, 31] immunosuppressive,[32] exhibits low neoantigen expression levels,[33] and high relapse rates. The continued challenges facing treatments for this patient population highlight a need for better control over the treatments and the immune responses they generate. An important goal of our study is to extend the benefits of the CpG-PBNP-based nanoimmunotherapy for the treatment of neuroblastoma.

There have been a few published reports, including ours, that describe the combination of PTT with immunotherapies for the treatment of cancer, including the use of CpG-coated nanoparticles utilized for PTT. These include hollow gold nanoshells,[34] CpG-loaded MoS_2 nanosheets,[35] graphene oxide,[36] Al_2O_3 nanoparticles,[37] and hollow CuS nanoparticles[5]. Compared with earlier studies, our work is distinct for the following reasons: 1) Prussian blue is a United States FDA-approved material as Radiogardase® and listed as an essential medicine by the World Health Organization as a radioactive poisoning antidote,[38] which indicates the safety of working with PBNPs, 2) PBNPs are biodegradable,[9] which mitigates concerns associated with the long-term fate and associated toxicities of nanoparticles within the body,[39] 3) we describe a facile method for coating CpG onto the PBNPs that enables the simultaneous delivery of tumor cell death, antigenicity, and adjuvanticity in a single nanoparticle, and 4) PBNPs combined with toll-like receptor agonists have not previously been applied to treat neuroblastoma.

We present a layer-by-layer scheme for the generation of the CpG-PBNPs, leveraging our expertise in generating polyelectrolyte multilayers.[7, 40-42] The properties of the resultant CpG-PBNPs are characterized for size, stability, absorption spectrum, and cytotoxicity. Next, we present the photothermal heating characteristics of the nanoparticles as well their immunostimulatory properties *in vitro* and *ex vivo*. Finally we test the efficacy of our CpG-PBNP-PTT in treating mice bearing syngeneic Neuro2a neuroblastoma tumors.

Experimental Section

Materials and chemicals

All synthesis procedures were conducted using ultrapure water obtained from a Milli-Q system (Millipore Corporation, Billerica, MA) with resistivity of 18.2 MΩ·cm. Potassium hexacyanoferrate (II) trihydrate (MW 422.39; $K_4[Fe(CN)_6]\cdot 3H_2O$), iron (III) chloride hexahydrate (MW 270.3; $Fe(Cl)_3\cdot 6H_2O$), and citric acid were purchased from Sigma-Aldrich (St. Louis, MO, USA), and were used as supplied. Acetone, ethanol, and ethidium bromide (EtBr) solution were obtained from Sigma-Aldrich. Poly(ethylenimine) (PEI, Mw 2,000, Mn 1,800, 50% w/v in H_2O) was purchased from Sigma-Aldrich, and diluted in acetate buffer (pH 5.2, Sigma-Aldrich). Murine CpG oligodeoxynucleotide (CpG) TLR9 ligand (ODN 1585; Class A)) was purchased from InVivoGen (San Diego, CA, USA). Fluorescent antibodies against HMGB1 and calreticulin were purchased from Abcam (Cambridge, UK). Lipopolysaccharide (LPS) was purchased from Thermo Fisher Scientific (Carlsbad, CA, USA).

Cells and cell culture

The murine neuroblastoma cell line Neuro2a was obtained from ATCC (Manassas, VA, USA) and cultured in Eagle's Minimum Essential Medium (EMEM) (Gibco, Carlsbad, CA, USA) containing 10% fetal bovine serum (FBS, Gibco) and 1% penicillin/streptomycin (Sigma-Aldrich). For *ex vivo* studies, splenic dendritic cells (DCs) were supplemented with RPMI 1640 medium (Lonza Bioscience, Manchester UK), supplemented with 10% FBS (Corning Inc., Corning, NY, USA), 2 mM L-glutamine (Gibco), 55 μM β-mercaptoethanol (Sigma-Aldrich) 1× non-essential amino acids (Fisher Scientific, Waltham, MA, USA), 10 mM HEPES (Fisher Scientific), and 0.5% penicillin/streptomycin (Gibco).

Animals

All animal studies were approved by the Institutional Animal Care and Use Committee of the George Washington University, Washington, DC, USA (Protocol # A396) and the University of Maryland, College Park, MD, USA. The studies were conducted to ensure humane care of the animals as per the institutional IACUC guidelines. For the DC activation studies, female C57BL/6J mice were obtained from Jackson Laboratory (Bar Harbor, ME, USA). For T cell proliferation studies, female OT-I mice (C57BL/6-Tg(TcraTcrb)1100Mjb/K) were purchased from Jackson Laboratory. For *in vivo* studies, five week old, female A/J mice were purchased from Jackson Laboratory. The animals were acclimated for 3-4 days prior to tumor inoculation.

Synthesis of PBNPs

PBNPs were synthesized using a one-pot synthesis scheme as previously described by us with minor modifications.[9, 18, 43, 44] Briefly, an aqueous solution of 1.0 mM $FeCl_3\cdot 6H_2O$ and 0.5 mmol citric acid in 20 mL of MilliQ water was added under vigorous stirring to an aqueous 20 mL solution containing 1 mM $K_4Fe(CN)_6\cdot 3H_2O$ and 0.5 mmol citric acid at 60 °C. After stirring for 1 minute, the solution was allowed to come to room temperature, and the precipitate containing PBNPs was isolated by the addition of equal volumes of acetone followed by centrifugation (10,400 ×g for 10 minutes). The collected PBNPs were rinsed and resuspended by sonication for 5 s using

a Q500 sonicator (QSonica LLC, Newton, CT, USA) at high power in Milli-Q water. The isolation and rinsing steps were repeated 3× before the stock nanoparticles were finally resuspended by sonication in Milli-Q water. The concentration of the PBNPs was determined by measuring the absorbance of the nanoparticle suspensions at 680 nm using a calibration curve plotting OD_{680} versus concentration of PBNPs in mg/mL. These calculations were confirmed by weighing a known volume of the PBNPs before and after drying in an oven.

Synthesis of CpG-PBNPs

To generate the CpG-PBNPs, we adopted a layer-by-layer coating strategy where PEI was first coated on to the PBNPs. PBNPs at a concentration of (3 mg/mL) were contacted with equal volumes of PEI (12 mg/mL) in acetate buffer (pH 5.2) at room temperature for 1 hour on an orbital shaker. The resultant PEI-coated PBNPs (PEI-PBNPs) were collected by centrifugation at 10,400 ×g for 10 minutes with the addition of equal volumes of ethanol. After 4 washes with the 50%-50% Milli-Q water-ethanol mixture, the PEI-PBNPs were resuspended by sonication in Milli-Q water. The concentration of the PEI-PBNPs was determined as described above. Next, CpG was assembled on the PEI-PBNPs. Accordingly, 300 µL of an aqueous solution of CpG (containing 100 µg CpG in endotoxin-free water) was added to 500 µL of the above PEI-PBNP suspension (at a concentration of 2 mg/mL) under stirring at room temperature for 15 minutes. The mixture was centrifuged at 21,000 ×g for 15 minutes to collect the CpG-PBNPs. The amount of CpG loaded on to the nanoparticles was calculated by measuring the difference in absorbance (at 260 nm) between the CpG added to the nanoparticles and the CpG detected in the nanoparticle-free supernatant, using a NanoDrop spectrophotometer (Thermo Fisher Scientific). Based on these measurements, we calculated the entrapment efficiency (%EE) = (Amount of CpG added – Amount of CpG measured in the supernatant)/(Amount of CpG added).

Nanoparticle characterization

The size (hydrodynamic diameter) and charge (zeta potential) distributions of PBNPs, PEI-PBNPs and CpG-PBNPs were measured using dynamic light scattering (DLS) on a Zetasizer Nano ZS (Malvern Instruments, Malvern, UK). The visible-NIR (Vis-NIR) absorbance spectra of the nanoparticles were measured on the Genesys 10S spectrophotometer using the VISIONlite software (Thermo Fisher Scientific). Transmission electron microscopy (TEM) images of the PBNPs, PEI-PBNPs, and CpG-PBNPs were prepared by loading 5 µL of the nanoparticle suspensions on to formvar carbon coated copper grids (Ted Pella, Inc., Reading CA) and dried overnight. The samples were imaged in a Talos F200X Transmission Electron Microscope (TEM) (Thermo Fisher) at 200 KV. The Velox software (Thermo Fisher) captured images at 200X magnification with a Ceta 4k x 4k camera. Multiday stability of the nanoparticles in ultrapure water was assessed by measuring their hydrodynamic size distributions, zeta potentials, and Vis-NIR spectra every 24 hours over 7 days.

Release of CpG from CpG-PBNPs

To quantify if CpG is tightly bound on the layer-by-layer-assembled CpG-PBNPs, EtBr was added to CpG-PBNPs or dose-matched free CpG at a 1:5 mass ratio and allowed to equilibrate for 1 hour. Fluorescence was measured on a Gemini XPS plate reader (Molecular Devices LLC, San Jose, CA, USA) at an excitation wavelength of 520 nm and an emission wavelength of 590 nm. The intensity ratio was calculated by comparing the fluorescence of the CpG-PBNPs with EtBr to the fluorescence of CpG and EtBr alone. To determine the multi-day release of CpG from the nanoparticles at varying physiological pHs (4.6, 7.0, and 8.0), the appropriate amounts of mild acid or base were added to the CpG-PBNP suspensions (0.8 mg/mL) in Milli-Q water until the desired, stable pH was obtained. The amount of CpG released was measured using a NanoDrop spectrophotometer. To determine the amount of CpG released from the particles, PTT was conducted as a function of concentration (0.1 mg/mL and 0.5 mg/mL) at a fixed laser power of 0.75 W for 10 minutes. The PTT capabilities were also tested as a function of laser power (0.25, 0.75, and 1.25 W) by irradiating CpG-PBNPs at a fixed concentration of 1 mg/mL. EtBr was added to the nanoparticles after PTT or dose-matched free CpG as described above.

Cell viability assays

Intrinsic and PTT-induced cytotoxicity of the CpG-PBNPs *in vitro* was measured using the murine neuroblastoma cell line Neuro2a. Briefly, Neuro2a was seeded in a 96-well plate at a cell density of 50,000 cells per well, and incubated with either vehicle or varying concentrations of nanoparticles (0.001-0.5 mg/mL) with or without laser irradiation using an 808 nm NIR continuous wave, collimated diode laser (Laserglow Technologies, Toronto, ON, Canada) at 1.5 W/cm^2 for 10 minutes. Twenty-four hours after the treatment, cell viability was assessed using the CellTiter-Glo luminescent cell viability assay (Promega Corporation, Madison, WI, USA). Each treatment was conducted with at least three replicates.

***In vitro* PTT**

The photothermal capabilities of CpG-PBNPs were tested *in vitro* as a function of concentration by varying the concentration of the nanoparticles from 0.025 mg/mL to 0.5 mg/mL at a fixed laser power of 0.75 W for 10 minutes. The PTT capabilities were also measured as a function of laser power (0.25W – 1.25W) by irradiating CpG-PBNPs at a fixed concentration of 1 mg/mL for 10 minutes. The stability of the nanoparticles as a photothermal agent was assessed by a cyclic heating/cooling study where 1 mg/mL CpG-PBNPs were irradiated by the NIR laser at 0.75 W (laser on/off times = 10 minutes each). The laser power administered in each study was confirmed using a power meter (Thorlabs, Newton, NJ, USA). Temporal temperature measurements were taken using an i7 thermal imaging camera (FLIR, Arlington, VA, USA).

***Ex vivo* DC Studies**

DCs were isolated from the spleens of naïve C57BL/6J mice using a CD11c positive magnetic isolation kit, according to the manufacturer's instructions (Miltenyi Biotec GmbH, Bergisch Gladbach, Germany). Cells were plated (10^5 cells/well) in RPMI 1640 media described above. Samples, which were added in triplicate, included media, LPS (1 μg/mL), CpG (40, 10 and 1 μg/mL), PBNPs (1 – 0.25 mg/mL, in 2× dilutions), and CpG PBNPs (1 – 0.25 mg/mL, in 2× dilutions). Cultures were incubated for 24 hours, then collected by centrifugation (800 ×g, 5 minutes), washed twice in FACS buffer, and blocked with anti-CD16/CD32 (BD Biosciences, Franklin Lakes, NJ, USA). The cells were finally stained for 20 minutes at room temperature using monoclonal antibodies against the surface activation markers CD40, CD80, and CD86 (BD Biosciences). After staining, cells were washed twice and resuspended in FACS buffer containing DAPI for analysis by flow cytometry (CantoII, BD Biosciences). All flow cytometry data were collected and analyzed using FlowJo software (Tree Star Inc., Ashland, OR, USA).

***Ex vivo* T cell proliferation studies**

$CD11c^+$ DCs from naïve C57BL/6J mice were isolated and treated as described above for DC activation studies. All treatment groups received either free Trp2 peptide (1.25 ng/well) or no Trp2. After 48 h of culture, Trp2-specific $CD8^+$ T cells were isolated by negative magnetic separation (StemCell Technologies, Vancouver, Canada) from the spleens of Trp2 transgenic mice (A gift from Dr. Giorgio Trinchieri, NCI, NIH). Isolated $CD8^+$ T cells were stained with eFluor 647 proliferation dye (10 nM) and washed 3 times, then 3×10^5 labeled T cells were added to the DC cultures. After another 48 hours of co-culture, cells were washed and blocked, as described above. Cells were then stained with anti-CD8 (BD Biosciences, Franklin Lakes, NJ, USA) for 20 min at room temperature, washed, and resuspended in DAPI in FACS buffer for analysis by flow cytometry.

ICD marker analysis

In vitro CpG-PBNP-PTT and PBNP-PTT was performed as described above (using equivalent concentrations of nanoparticles or controls with/without laser irradiation).[19] Cell suspensions were then washed and stained with fluorescent antibodies against HMBG1 (intracellular) and calreticulin (extracellular), and flow cytometry was performed. Flow cytometry was performed on the FACSCaliber (BD Biosciences), and analysis was done using the FlowJo software. For intracellular ATP presence, cells were washed after *in vitro* PTT and the CellTiter-Glo luminescent cell viability assay was performed.

***In vivo* studies**

For establishing a murine neuroblastoma model, one million Neuro2a cells suspended in phosphate-buffered saline were injected subcutaneously in the shaved backs of 4-6 week old female A/J mice, as previously described.[9, 19] All the treatments commenced after the tumors reached a diameter of at least 5 mm (~60 mm^3). Mice were anesthetized prior to and during treatment using 5% isoflurane. Tumor-bearing mice were divided into five groups (n=10 mice/ group): 1) Vehicle (no treatment, injected intratumorally with 50 μL PBS on day 0), 2) Free CpG (10 μg CpG injected intratumorally on days 0, 2, and 5), 3) CpG-PBNPs (2 μg conjugated on the PBNPs; injected intratumorally on days 0, 2, and 5), 4) PBNP-PTT (50 μL of 1 mg/mL PBNPs intratumorally, irradiated at 0.75 W for 10 minutes), and 5) CpG-PBNP-PTT nanoimmunotherapy (50 μL of 1 mg/mL CpG-PBNPs, 2 μg bound CpG, irradiated at 0.75 W for 10 minutes, CpG-PBNPs boosts were given (without PTT) on days 2 and 5). Temperatures reached during PTT were measured using the i7 FLIR thermal imaging camera. Tumor growth was monitored following inoculation and treatments by routine caliper measurements. Surviving mice were rechallenged 60-90 days after treatment with one million Neuro2a cells as described above to assess if the surviving animals developed immunological memory.

Animal exclusion and euthanasia criteria

Animals were excluded from the study if their tumors failed to grow after Neuro2a inoculation. This exclusion occurred infrequently because greater than 95% of injected mice developed tumors. A tumor size of 15 mm diameter in any dimension was designated as the endpoint and mice were euthanized at that time. Euthanasia was achieved through cervical dislocation after CO_2 narcosis. If the tumor impaired mobility of the animal, became ulcerated or appeared infected, or if the mice displayed any signs of distress such as assuming a sick mouse posture, the mice were immediately removed from the study and euthanized. All these steps were conducted in accordance with the approved IACUC protocols. A similar protocol was followed for the tumor rechallenge studies.

Statistical analysis

Statistical significance was determined from a two-tailed Student's t test and values with $p < 0.05$ qualified as statistically significant. Survival results were analyzed according to a Kaplan-Meier curve. The log-rank test was used to determine statistically significant differences in survival between the various groups.

Results

Layer-by-layer coating yields CpG-PBNPs with stable, monodisperse size distributions that retain the absorption properties of PBNPs and are not cytotoxic

We employed a layer-by-layer coating scheme to generate the CpG-PBNPs by sequentially coating the PBNPs with PEI and then CpG. Using this coating scheme, the yield of PEI-PBNPs was 92% on a mass/mass basis (gram of PEI-PBNPs obtained per gram PBNPs used in the coating) and the yield of CpG-PBNPs was 99.5% (gram of CpG-PBNPs obtained per gram of

PEI-PBNPs used in the coating) resulting in an overall process yield of approximately 91.5% (g CpG-PBNP/g PBNP). We measured the size, zeta potential, and Vis-NIR spectrum of the resultant CpG-PBNPs to assess their properties relative to unmodified PBNPs and PEI-PBNPs, to ensure that coating PBNPs with CpG did not affect the intrinsic characteristics of PBNPs. DLS measurements yielded CpG-PBNP size distributions that were similar to PBNPs and intermediate PEI-PBNPs (mean diameter ~ 190 nm; Figure 2A). Further, we were able to verify that the layer-by-layer coating was able to successfully coat the PBNPs with PEI and then CpG using zeta potential measurements (Figure 2B). Specifically, the intrinsic negative charge of PBNPs (average zeta potential -34 mV) changed to a net positive charge upon addition of positively charged PEI (+42 mV) and then back to a net negative charge after subsequent addition of the negatively charged CpG (-32 mV). The Vis-NIR spectrum of CpG-PBNPs demonstrated an absorption band between 650 and 900 nm (λmax = 705 nm; Figure 2C), which is similar to the absorption band of unmodified PBNPs.[9, 17, 18] This absorption band corresponds to the energy of the metal-to-metal charge transfer between Fe^{II} and Fe^{III} through the cyanide bridge and confers photothermal heating capabilities to the nanoparticles (upon NIR laser irradiation). TEM images of PBNPs, PEI-PBNPs, and CpG-PBNPs showed the characteristic cuboidal morphology of PBNPs (Figure 2D). In contrast, the crystallinity of the PEI-PBNPs and CpG-PBNPs were less well-defined and diffuse compared with PBNPs. This could be attributed to the presence of the polymer layers on the PEI-PBNPs and CpG-PBNPs that were likely affected and/or damaged by exposure to the electron beam during the TEM imaging (Figures 2E and F). Using these synthesis conditions, the entrapment efficiency (%EE) for CpG in the CpG-PBNPs was approximately 25%, which corresponded to approximately 40 μg CpG/mg of nanoparticles.

We conducted a temporal DLS study to assess nanoparticle size distributions as a function of time. The nanoparticles (PBNPs, PEI-PBNPs, and CpG-PBNPs) were stable over 7 days as measured by consistent size distributions over the study (Figures 2G, 2H, and S1A). The addition of varying concentrations of PBNPs, PEI-PBNPs, or CpG-PBNPs (0.001-0.1 mg/mL) to Neuro2a cells did not significantly affect their cellular viability (Figures 2I and S1B), indicating biocompatibility of the nanoparticles within these concentration ranges. These results demonstrate that our synthesis scheme yields stable CpG-PBNPs with monodisperse size distributions that retain the Vis-NIR absorption properties and biocompatibility of uncoated PBNPs.

CpG-PBNPs retain the photothermal therapy capabilities of PBNPs after CpG coating

To assess the effect of the CpG coating on the photothermal heating properties of the resultant CpG-PBNPs, we conducted photothermal heating studies *in vitro* as a function of nanoparticle concentration, laser power, and cyclic heating (Figure 3). The photothermal heating effect was concentration-dependent (Figure 3A) and laser power-dependent (Figure 3B). The temperatures increased with increasing CpG-PBNP concentrations (0.025 to 0.5 mg/mL CpG-PBNPs) reaching a maximum temperature around 80 °C at 10 minutes at a concentration of 0.5 mg/mL CpG-PBNPs (laser power 0.75 W). The photothermal heating effect was also dependent on incident laser power, and was observed to increase with increasing laser powers (0.25 to 1.25 W) reaching a maximum temperature around 80 °C (for 1 mg/mL CpG-PBNPs) at 1.25 W at 10 minutes. Furthermore, we demonstrated the stability of CpG-PBNPs as PTT agents through a cyclic heating study (1 mg/mL CpG-PBNPs, 0.75 W laser power). CpG-PBNPs showed consistent photothermal heating tracing similar heating-cooling curves over three consecutive heating and cooling cycles indicating stability of the CpG-PBNPs as PTT agents (Figure 3C). To test the efficacy of CpG-PBNPs to induce Neuro2a killing, we tested cell viability at different concentrations of CpG-PBNPs with and without laser. Neuro2a cell viability significantly decreased as temperatures induced by CpG-PBNP-PTT increased (Figure 3D). These results show that coating PBNPs with CpG does not affect their photothermal heating abilities and indicate their suitability for use at PTT agents.

CpG-PBNPs contain tightly bound CpG and exhibit pH-dependent CpG release

We conducted studies to quantify the release of CpG from CpG-PBNPs because the release (or retention) of this immunological adjuvant from the nanoparticles directly impacts tumor adjuvanticity. An EtBr assay conducted to determine the binding affinity of CpG and the PBNPs demonstrated that only 6.75% of bound CpG in the CpG-PBNPs could complex with EtBr when compared with equivalent concentrations of free CpG (Figure 4A). This finding suggests that greater than 93% of CpG is tightly bound in the CpG-PBNPs post-synthesis. Complementary to these studies, we assessed the percentage of CpG that remained bound on the CpG-PBNPs as a function of varying pH and duration of contact. This is because we administer the CpG-PBNPs intratumorally for PTT and both tumor insterstitia and endosomal compartments - potential loci for the nanoparticles after intratumoral injection - exhibit mildly acidic pH compared to neutral, physiological pH observed in the serum and cytosol.[45, 46] At a neutral pH (7.0), the percent of bound CpG remained constant for up to 4 days and then decreased slightly (to 74.5%; Figure 4B). At a mildly acidic pH (4.6), the percent of bound CpG decreased slightly to 88.6% by Day 4 and down to 54.3% by Day 7. In contrast, at a mildly basic pH (8.0), the bound CpG decreased rapidly to 31.4% by Day 4 and was almost completely released by Day 7 at this pH. We can attribute this CpG release at mildly basic pHs to the well-described attack of the characteristic Fe^{II}-CN-Fe^{III} bonds of PBNPs (and CpG-PBNPs) by the slight excess of hydroxyl ions, previously described by us and others.[9, 47, 48] To test the fraction of CpG released from the nanoparticles after PTT, we conducted PTT at varying laser powers (0.25 W – 1.25 W), as

well as different concentrations (0.1 mg/mL – 0.5 mg/mL), reaching final temperatures of around 40°C, 60°C, and 80°C (Figure S2). EtBr was added as described above. Our results showed that CpG remained bound to the nanoparticles after PTT, regardless of temperatures attained under the various PTT conditions suggesting that heat did not cause the de-complexation of CpG from the nanoparticles (Figure 4C). Together, these studies demonstrate that CpG in the CpG-PBNPs, as synthesized, is tightly bound and remains tightly bound in the pH 4.6-7.0 range for up to 4 days, and after PTT, thus establishing the conditions for the retention of this adjuvant after intratumoral administration.

CpG-PBNPs activate DCs and cause CD8+ T cell proliferation *ex vivo*

To test the immunostimulatory properties of the CpG-PBNPs, we measured their ability to activate DCs and T cells compared to free CpG, PBNPs without CpG, and other controls *ex vivo* (Figures 5 and S3). First, we cultured splenic DCs with CpG-PBNPs or PBNPs at different concentrations (diluted 1x – 4x; 1-0.25 mg/mL), free CpG (low, medium, high concentrations; 1-40 μg/mL), LPS, or media, and assessed DC activation by measuring expression of common DC surface activation markers: CD80, CD86, and CD40. Untreated DCs served as a negative control, while LPS and free CpG were employed as positive controls. The concentration of free CpG added to the DCs (e.g. 1×; 40 μg/mL) was equivalent to the amount of CpG bound on 1 mg/mL CpG-PBNPs (40 μg CpG/mg of nanoparticle). Flow cytometry analysis demonstrated increased activation of DCs by CpG-PBNPs compared to uncoated PBNPs as measured by their increased CD80, CD86, and CD40 expression levels (Figures 5A and S3A). DC activation was also observed to be dose-dependent, increasing with higher concentrations of CpG-PBNPs. In contrast, DC activation with varying concentrations of PBNPs was constant at levels similar to those observed for the untreated DCs (media; negative control). Furthermore, the CD80/86 activation levels with the various doses of CpG-PBNPs were similar to those observed for free CpG. Importantly, the percentage of CD11c+ live cells were similar across all treatment groups indicating biocompatibility of our nanoparticles (Figure S3B). These findings demonstrate that the CpG-PBNPs can activate DCs, as a result of the CpG coating.

In addition to the above studies, we tested the ability of the CpG-PBNPs to activate T cells. For these studies, we utilized Trp2 as a model antigen, expressed in several murine and human cancers, to test T cell activation in context of DC activation (via the CpG-PBNPs) and antigen-presentation (via the added Trp2) It is important to note here that while Trp2 is not expressed in neuroblastoma, it serves as a useful and well-characterized model antigen to test the immunostimulatory properties of the CpG-PBNPs. DCs that were activated by the same groups used in Figure 5A were co-cultured with Trp2-specific CD8+T cells (Figures S3C and D), in the presence of the Trp2 peptide (1.25 ng/well). We observed that when DCs activated by CpG-PBNPs were co-cultured with CD8+T cells in the presence of Trp2, their proliferation was increased compared to DCs activated with PBNP (at the same concentration) as measured by the T cell proliferation assay (Figure 5B). Furthermore, DCs activated with CpG-PBNPs were able to activate CD8+ T cells in a manner similar to DCs activated with free CpG (% proliferated was ~50% for both the 1 mg/mL CpG-PBNPs and the 40 μg/mL free CpG treatments). Overall, these results demonstrate the potential of the CpG-PBNPs to increase DC activation and T cell proliferation, which is important for overcoming tumor-mediated immunosuppression, and improving antitumor immune responses of a therapy.

CpG-PBNP-PTT elicits ICD in Neuro2a cells *in vitro*

As part of our multimodal therapy strategy, the CpG-PBNPs should not only activate DCs and T cells (via the CpG coating), but also cause trigger tumor cell death in a manner that engages the immune system (after PTT). These combined effects facilitate improved antigen processing and presentation, leading to enhanced antitumor effects.[16] Previously, we demonstrated the PBNP-PTT elicits ICD as measured by its biochemical correlates (released ATP and HMGB1, and increased surface calretriculin).[19] Here, we verify whether CpG-PBNP-PTT elicits ICD in Neuro2a cells. Specifically, we assessed the expression of ICD markers (ATP, HMGB1, and calreticulin) on Neuro2a cells treated with CpG-PBNP-PTT (Figure 6). CpG-PBNP-PTT caused a decrease in intracellular ATP levels in Neuro2a cells (similar to PBNP-PTT), which was lower than the ATP levels observed in Neuro2a cells treated with the vehicle, laser alone, PBNPs, or CpG-PBNPs (Figure 6A). CpG-PBNP-PTT also triggered a significant increase in surface calreticulin expression (similar to PBNP-PTT) relative to the aforementioned treatment groups (Figure 6B). Finally, CpG-PBNP-PTT caused a significant decrease in intracellular HMGB1 levels (>40% decrease; similar to PBNP-PTT) compared to the other treatment groups. These findings suggest the CpG-PBNP-PTT is able to effectively elicit ICD in treated Neuro2a cells thus priming a favorable antitumor immune response via this endogenous adjuvant release.

CpG-PBNP-PTT nanoimmunotherapy results in complete tumor regression, long-term survival, and rejection of tumor rechallenge in a mouse model of neuroblastoma

Building on our findings described above, we next tested if the increased antigenicity and adjuvanticity elicited by CpG-PBNP-PTT generated anti-tumor immunity in a syngeneic murine model of neuroblastoma. Neuro2a neuroblastoma tumor-bearing mice were divided into five treatment groups (n = 10/group; Figure 7A): 1) Vehicle (PBS), 2) Free CpG, 3) CpG-PBNPs, 4) PBNP-PTT, and 5) CpG-PBNP-PTT. The average final tumor temperatures achieved during PTT measured by the thermal imaging camera was ~60 ^{o}C (Figure 7B), which corresponded to the temperature range needed to elicit ICD in Neuro2a-bearing mice.[19] CpG-PBNP-PTT resulted in complete tumor regression in the majority of treated mice (7/10)

compared to mice in the four other treatment groups (0/10 each in the vehicle-treated, Free CpG-treated, and the PBNP-PTT-treated groups, and 1/10 in the CpG-PBNPs-treated group; Figure S4). More importantly, CpG-PBNP-PTT resulted in long-term survival (survival >60 days post-treatment) in 70% of the treated tumor-bearing mice, which was significantly higher than the long-term survival observed in tumor-bearing mice in all other treatment groups (Figure 7C; $p < 0.05$; log-rank test).

We then tested if CpG-PBNP-PTT conferred protection against tumor rechallenge in long-term surviving mice (Figure 7D). Our studies consisted of two groups: 1) Naïve group, where untreated mice were challenged with 10^6 Neuro2a cells, and 2) Rechallenged group: where long-term surviving, CpG-PBNP-PTT-treated mice where rechallenged with 10^6 Neuro2a cells after at least 60 days of tumor-free survival ($n \geq 7$/group for this study). Remarkably, all the long-term surviving mice that were CpG-PBNP-PTT-treated, exhibited protection against the tumor rechallenge, and these mice rapidly eliminated the rechallenged tumors compared with naïve mice that exhibited rapid tumor progression. Further, mice in this rechallenged group survived for >60 days post tumor rechallenge compared with naïve mice that had to be euthanized due to high tumor burden 12-14 days post-challenge. Taken together, these data suggest the importance of increasing tumor antigenicity and adjuvanticity via the CpG-PBNP-PTT nanoimmunotherapy in conferring complete tumor-regression, long-term survival, and protection against tumor rechallenge in the mouse model of neuroblastoma.

Discussion

We have described a novel CpG-PBNPs nanoimmunotherapy that triggers robust antitumor immune responses in a syngeneic model of neuroblastoma by combining the effects of nanoparticle-based photothermal therapy with increased tumor antigenicity and adjuvanticity (Figure 1). We employed a layer-by-layer coating scheme to generate stable, monodisperse, and biocompatible CpG-PBNPs wherein CpG was tightly bound to the nanoparticles (Figures 2 and 4). Layer-by layer assembly has been used to coat a wide range of substrates with polyelectrolyte multilayers consisting of antigens, adjuvants, or both antigen and adjuvant.[7, 41, 49-53] Similarly, the synthesis and coating scheme described here can be easily modified to coat PBNPs with other immune signals consisting of tumor antigen, immunological adjuvants, and/or other antigen-adjuvants combinations. This tripartite PTT-based cell death-antigenicity-adjuvanticity can, in principle, be applied for the treatment of other solid tumors that employ similar immune evasion mechanisms. The CpG coating on the CpG-PBNPs was able to increase activation of DC and the proliferation of CD8+ T cells in the presence of a model Trp2 antigen *ex vivo* (Figure 5). Increasing antigen presentation and activation of antigen-specific T cell responses is crucial in overcoming tumor-mediated immunosuppression. The CpG-PBNPs retained the PTT properties of PBNPs (Figure 3) and were able to elicit immunogenic cell death in treated Neuro2a neuroblastoma cells (Figure 6), effects important in initiating a robust antitumor immune response. Although our study focused on the effects of CpG-PBNP-PTT on tumor cell death, antigenicity, and adjuvanticity, one cannot discount the importance of evaluating the effects of our therapy on other immune cell subsets, including NK cells, macrophages (M1 and M2 phenotypes), and suppressor cells (Tregs, MDSCs) to get a more complete picture of the associated effects of our therapy. These studies are either ongoing or will be undertaken by our group in the near future. The CpG-PBNP-PTT nanoimmunotherapy was able to elicit complete tumor regression, long-term survival, and protection against tumor rechallenge in a majority of Neuor2a tumor-bearing mice (Figure 7). While these results are extremely encouraging, additional studies need to be performed in animal models of disseminated neuroblastoma to better mimic neuroblastoma risk groups associated with a poor prognosis (high-risk neuroblastoma), and these are the focus of several ongoing studies.

Conclusions

We have described a nanoimmunotherapy for treating cancer using CpG-PBNPs that leverages the ablative properties of PBNPs and the immunostimulatory properties of CpG oligodeoxynucleotides. Our nanoimmunotherapy increases antigenicity and adjuvanticity of ablated tumors that results in complete tumor regression and long-term survival, strongly suggesting the importance of these phenomena for engaging a robust antitumor immune response and improved treatment outcomes.

Conflicts of Interest

C.M.J. is an employee of the Maryland Veterans Affairs (VA) Health Care System at the Baltimore VA Medical Center. The views reported in this paper do not reflect the views of the Department of Veterans Affairs or the United States Government. C.M.J. holds an equity position in Cellth Systems, LLC.

Acknowledgements

This work was supported by the Alex's Lemonade Stand Foundation for Childhood Cancer's 'A' Award, the George Washington University Cancer Center, and the University of Maryland College Park. This work was supported in part by the United States Department of Veteran Affairs (#1I01BX003690), the Damon Runyon Foundation (#DRR3415), NSF CAREER Award (#1351688), and Alliance for Cancer Gene Therapy (#15051543). M.L.B. is a trainee of the NIH T32 Host-Pathogen Interaction Fellowship (#AI089621). Research reported in this publication was supported in part by the National Cancer Institute of the National Institutes of Health under Award Number R37CA226171. The content is solely the responsibility of the authors and does not necessarily represent the official views of the National Institutes of Health.

References

1. C. Loo, A. Lowery, N. Halas, J. West and R. Drezek, *Nano letters*, 2005, **5**, 709-711.
2. D. K. Roper, W. Ahn and M. Hoepfner, *J Phys Chem C Nanomater Interfaces*, 2007, **111**, 3636-3641.
3. X. Huang, P. K. Jain, I. H. El-Sayed and M. A. El-Sayed, *Lasers in medical science*, 2008, **23**, 217-228.
4. A. S. Bear, L. C. Kennedy, J. K. Young, S. K. Perna, J. P. Mattos Almeida, A. Y. Lin, P. C. Eckels, R. A. Drezek and A. E. Foster, *PLoS One*, 2013, **8**, e69073.
5. L. Guo, D. D. Yan, D. Yang, Y. Li, X. Wang, O. Zalewski, B. Yan and W. Lu, *ACS Nano*, 2014, **8**, 5670-5681.
6. C. Wang, L. Xu, C. Liang, J. Xiang, R. Peng and Z. Liu, *Adv Mater*, 2014, **26**, 8154-8162.
7. P. Zhang, Y. C. Chiu, L. H. Tostanoski and C. M. Jewell, *ACS Nano*, 2015, **9**, 6465-6477.
8. R. A. Burga, S. Patel, C. M. Bollard, Y. C. CR and R. Fernandes, *Nanomedicine (Lond)*, 2016, **11**, 1759-1767.
9. J. Cano-Mejia, R. A. Burga, E. E. Sweeney, J. P. Fisher, C. M. Bollard, A. D. Sandler, C. R. Y. Cruz and R. Fernandes, *Nanomedicine Nanotechnol Biol Med*, 2017, **13**, 771-781.
10. M. A. Postow, M. K. Callahan, C. A. Barker, Y. Yamada, J. Yuan, S. Kitano, Z. Mu, T. Rasalan, M. Adamow, E. Ritter, C. Sedrak, A. A. Jungbluth, R. Chua, A. S. Yang, R. A. Roman, S. Rosner, B. Benson, J. P. Allison, A. M. Lesokhin, S. Gnjatic and J. D. Wolchok, *N Engl J Med*, 2012, **366**, 925-931.
11. Y. Min, K. C. Roche, S. Tian, M. J. Eblan, K. P. McKinnon, J. M. Caster, S. Chai, L. E. Herring, L. Zhang, T. Zhang, J. M. DeSimone, J. E. Tepper, B. G. Vincent, J. S. Serody and A. Z. Wang, *Nat Nanotechnol*, 2017, **12**, 877-882.
12. L. Galluzzi, I. Vitale, S. A. Aaronson, J. M. Abrams, D. Adam, P. Agostinis, E. S. Alnemri, L. Altucci, I. Amelio, D. W. Andrews, M. Annicchiarico-Petruzzelli, A. V. Antonov, E. Arama, E. H. Baehrecke, N. A. Barlev, N. G. Bazan, F. Bernassola, M. J. M. Bertrand, K. Bianchi, M. V. Blagosklonny, K. Blomgren, C. Borner, P. Boya, C. Brenner, M. Campanella, E. Candi, D. Carmona-Gutierrez, F. Cecconi, F. K. Chan, N. S. Chandel, E. H. Cheng, J. E. Chipuk, J. A. Cidlowski, A. Ciechanover, G. M. Cohen, M. Conrad, J. R. Cubillos-Ruiz, P. E. Czabotar, V. D'Angiolella, T. M. Dawson, V. L. Dawson, V. De Laurenzi, R. De Maria, K. M. Debatin, R. J. DeBerardinis, M. Deshmukh, N. Di Daniele, F. Di Virgilio, V. M. Dixit, S. J. Dixon, C. S. Duckett, B. D. Dynlacht, W. S. El-Deiry, J. W. Elrod, G. M. Fimia, S. Fulda, A. J. Garcia-Saez, A. D. Garg, C. Garrido, E. Gavathiotis, P. Golstein, E. Gottlieb, D. R. Green, L. A. Greene, H. Gronemeyer, A. Gross, G. Hajnoczky, J. M. Hardwick, I. S. Harris, M. O. Hengartner, C. Hetz, H. Ichijo, M. Jaattela, B. Joseph, P. J. Jost, P. P. Juin, W. J. Kaiser, M. Karin, T. Kaufmann, O. Kepp, A. Kimchi, R. N. Kitsis, D. J. Klionsky, R. A. Knight, S. Kumar, S. W. Lee, J. J. Lemasters, B. Levine, A. Linkermann, S. A. Lipton, R. A. Lockshin, C. Lopez-Otin, S. W. Lowe, T. Luedde, E. Lugli, M. MacFarlane, F. Madeo, M. Malewicz, W. Malorni, G. Manic, J. C. Marine, S. J. Martin, J. C. Martinou, J. P. Medema, P. Mehlen, P. Meier, S. Melino, E. A. Miao, J. D. Molkentin, U. M. Moll, C. Munoz-Pinedo, S. Nagata, G. Nunez, A. Oberst, M. Oren, M. Overholtzer, M. Pagano, T. Panaretakis, M. Pasparakis, J. M. Penninger, D. M. Pereira, S. Pervaiz, M. E. Peter, M. Piacentini, P. Pinton, J. H. M. Prehn, H. Puthalakath, G. A. Rabinovich, M. Rehm, R. Rizzuto, C. M. P. Rodrigues, D. C. Rubinsztein, T. Rudel, K. M. Ryan, E. Sayan, L. Scorrano, F. Shao, Y. Shi, J. Silke, H. U. Simon, A. Sistigu, B. R. Stockwell, A. Strasser, G. Szabadkai, S. W. G. Tait, D. Tang, N. Tavernarakis, A. Thorburn, Y. Tsujimoto, B. Turk, T. Vanden Berghe, P. Vandenabeele, M. G. Vander Heiden, A. Villunger, H. W. Virgin, K. H. Vousden, D. Vucic, E. F. Wagner, H. Walczak, D. Wallach, Y. Wang, J. A. Wells, W. Wood, J. Yuan, Z. Zakeri, B. Zhivotovsky, L. Zitvogel, G. Melino and G. Kroemer, *Cell death and differentiation*, 2018, **25**, 486-541.
13. G. Kroemer, L. Galluzzi, O. Kepp and L. Zitvogel, *Annu Rev Immunol*, 2013, **31**, 51-72.
14. O. Kepp, L. Senovilla, I. Vitale, E. Vacchelli, S. Adjemian, P. Agostinis, L. Apetoh, F. Aranda, V. Barnaba, N. Bloy, L. Bracci, K. Breckpot, D. Brough, A. Buque, M. G. Castro, M. Cirone, M. I. Colombo, I. Cremer, S. Demaria, L. Dini, A. G. Eliopoulos, A. Faggioni, S. C. Formenti, J. Fucikova, L. Gabriele, U. S. Gaipl, J. Galon, A. Garg, F. Ghiringhelli, N. A. Giese, Z. S. Guo, A. Hemminki, M. Herrmann, J. W. Hodge, S. Holdenrieder, J. Honeychurch, H. M. Hu, X. Huang, T. M. Illidge, K. Kono, M. Korbelik, D. V. Krysko, S. Loi, P. R. Lowenstein, E. Lugli, Y. Ma, F. Madeo, A. A. Manfredi, I. Martins, D. Mavilio, L. Menger, N. Merendino, M. Michaud, G. Mignot, K. L. Mossman, G. Multhoff, R. Oehler, F. Palombo, T. Panaretakis, J. Pol, E. Proietti, J. E. Ricci, C. Riganti, P. Rovere-Querini, A. Rubartelli, A. Sistigu, M. J. Smyth, J. Sonnemann, R. Spisek, J. Stagg, A. Q. Sukkurwala, E. Tartour, A. Thorburn, S. H. Thorne, P. Vandenabeele, F. Velotti, S. T. Workenhe, H. Yang, W. X. Zong, L. Zitvogel, G. Kroemer and L. Galluzzi, *Oncoimmunology*, 2014, **3**, e955691.
15. S. Ladoire, D. Enot, F. Andre, L. Zitvogel and G. Kroemer, *Oncoimmunology*, 2016, **5**, e1082706.
16. L. Galluzzi, A. Buque, O. Kepp, L. Zitvogel and G. Kroemer, *Nat Rev Immunol*, 2017, **17**, 97-111.
17. G. Fu, W. Liu, S. Feng and X. Yue, *Chem Commun* 2012, **48**, 11567–11569.
18. H. A. Hoffman, L. Chakarbarti, M. F. Dumont, A. D. Sandler and R. Fernandes, *RSC Advances*, 2014, **4**, 29729-29734.
19. E. E. Sweeney, J. Cano-Mejia and R. Fernandes, *Small*, 2018, DOI: 10.1002/smll.201800678, e1800678.

20. A. F. Carpentier, L. Chen, F. Maltonti and J. Y. Delattre, *Cancer Res*, 1999, **59**, 5429-5432.
21. S. Pilon-Thomas, W. Li, J. J. Briggs, J. Djeu, J. J. Mule and A. I. Riker, *J Immunother*, 2006, **29**, 381-387.
22. S. Adams, *Immunotherapy*, 2009, **1**, 949-964.
23. L. Yang, L. Sun, X. Wu, L. Wang, H. Wei, M. Wan, P. Zhang and Y. Yu, *Clin Immunol*, 2009, **131**, 426-437.
24. L. Chakrabarti, T. Abou-Antoun, S. Vukmanovic and A. D. Sandler, *Frontiers in oncology*, 2012, **2**, 82.
25. L. Chakrabarti, B. D. Wang, N. H. Lee and A. D. Sandler, *PLoS One*, 2013, **8**, e83521.
26. L. Chakrabarti, C. Morgan and A. D. Sandler, *PLoS One*, 2015, **10**, e0129237.
27. E. Ward, C. Desantis, A. Robbins, B. Kohler and A. Jemal, *CA Cancer J Clin*, 2014, **64**, 83-103.
28. R. L. Siegel, K. D. Miller and A. Jemal, *CA Cancer J Clin*, 2018, **68**, 7-30.
29. F. Bellanti, B. Kågedal and O. Della Pasqua, *Eur J Clin Pharmacol*, 2011, **67 Suppl 1**, 87-107.
30. G. M. Brodeur, M. D. Hogarty, Y. P. Mosse and J. M. Maris, in *Principles and Practice of Pediatric Oncology*, eds. P. A. Pizzo and D. G. Poplack, Wolters Kluwer Health/Lippincott Williams & Wilkins, Philadelphia, PA, 6th edn., 2010, pp. 886-922.
31. T. J. Pugh, O. Morozova, E. F. Attiyeh, S. Asgharzadeh, J. S. Wei, D. Auclair, S. L. Carter, K. Cibulskis, M. Hanna, A. Kiezun, J. Kim, M. S. Lawrence, L. Lichenstein, A. McKenna, C. S. Pedamallu, A. H. Ramos, E. Shefler, A. Sivachenko, C. Sougnez, C. Stewart, A. Ally, I. Birol, R. Chiu, R. D. Corbett, M. Hirst, S. D. Jackman, B. Kamoh, A. H. Khodabakshi, M. Krzywinski, A. Lo, R. A. Moore, K. L. Mungall, J. Qian, A. Tam, N. Thiessen, Y. Zhao, K. A. Cole, M. Diamond, S. J. Diskin, Y. P. Mosse, A. C. Wood, L. Ji, R. Sposto, T. Badgett, W. B. London, Y. Moyer, J. M. Gastier-Foster, M. A. Smith, J. M. Guidry Auvil, D. S. Gerhard, M. D. Hogarty, S. J. Jones, E. S. Lander, S. B. Gabriel, G. Getz, R. C. Seeger, J. Khan, M. A. Marra, M. Meyerson and J. M. Maris, *Nature genetics*, 2013, **45**, 279-284.
32. V. Pistoia, F. Morandi, G. Bianchi, A. Pezzolo, I. Prigione and L. Raffaghello, *Frontiers in oncology*, 2013, **3**, 167.
33. T. N. Schumacher and R. D. Schreiber, *Science*, 2015, **348**, 69-74.
34. L. Luo, C. Zhu, H. Yin, M. Jiang, J. Zhang, B. Qin, Z. Luo, X. Yuan, J. Yang, W. Li, Y. Du and J. You, *ACS Nano*, 2018, **12**, 7647-7662.
35. Q. Han, X. Wang, X. Jia, S. Cai, W. Liang, Y. Qin, R. Yang and C. Wang, *Nanoscale*, 2017, **9**, 5927-5934.
36. Y. Tao, E. Ju, J. Ren and X. Qu, *Biomaterials*, 2014, **35**, 9963-9971.
37. W. Chen, M. Qin, X. Chen, Q. Wang, Z. Zhang and X. Sun, *Theranostics*, 2018, **8**, 2229-2241.
38. P. J. Faustino, Y. Yang, J. J. Progar, C. R. Brownell, N. Sadrieh, J. C. May, E. Leutzinger, D. A. Place, E. P. Duffy, F. Houn, S. A. Loewke, V. J. Mecozzi, C. D. Ellison, M. A. Khan, A. S. Hussain and R. C. Lyon, *Journal of pharmaceutical and biomedical analysis*, 2008, **47**, 114-125.
39. Y. Chen, L. Wu, Q. Wang, M. Wu, B. Xu, X. Liu and J. Liu, *Human & experimental toxicology*, 2016, **35**, 1123-1132.
40. Y. C. Chiu, J. M. Gammon, J. I. Andorko, L. H. Tostanoski and C. M. Jewell, *ACS applied materials & interfaces*, 2016, **8**, 18722-18731.
41. Y. C. Chiu, J. M. Gammon, J. I. Andorko, L. H. Tostanoski and C. M. Jewell, *ACS biomaterials science & engineering*, 2015, **1**, 1200-1205.
42. M. L. Bookstaver, K. L. Hess and C. M. Jewell, *Small*, 2018, **14**, e1802202.
43. J. M. Vojtech, J. Cano-Mejia, M. F. Dumont, R. W. Sze and R. Fernandes, *J Vis Exp*, 2015, DOI: 10.3791/52621, e52621.
44. E. E. Sweeney, R. A. Burga, C. Li, Y. Zhu and R. Fernandes, *Sci Reports*, 2016, **6**, 37035.
45. C. Song, R. Griffin and H. J. Park, in *Cancer Drug Discovery and Development: Cancer Drug Resistance*, ed. B. T. H. P. Inc., Totowa, NJ, 2006, pp. 21-42.
46. F. H. Meng, R. Cheng, C. Deng and Z. Y. Zhong, *Materials Today*, 2012, **15**, 436-442.
47. K. Itaya, H. Akahoshi and S. Toshima, *J Electrochem Soc*, 1982, **129**, 1498-1500.
48. A. A. Karyakin, *Electroanal*, 2001, **13**, 813-819.
49. S. De Koker, L. J. De Cock, P. Rivera-Gil, W. J. Parak, R. Auzely Velty, C. Vervaet, J. P. Remon, J. Grooten and B. G. De Geest, *Adv Drug Deliv Rev*, 2011, **63**, 748-761.
50. P. C. DeMuth, Y. Min, B. Huang, J. A. Kramer, A. D. Miller, D. H. Barouch, P. T. Hammond and D. J. Irvine, *Nature materials*, 2013, **12**, 367-376.
51. L. H. Tostanoski, Y. C. Chiu, J. I. Andorko, M. Guo, X. Zeng, P. Zhang, W. Royal, 3rd and C. M. Jewell, *ACS Nano*, 2016, DOI: 10.1021/acsnano.6b04001.
52. Q. Zeng, J. M. Gammon, L. H. Tostanoski, Y. C. Chiu and C. M. Jewell, *ACS biomaterials science & engineering*, 2017, **3**, 195-205.
53. M. L. Bookstaver, S. J. Tsai, J. S. Bromberg and C. M. Jewell, *Trends Immunol*, 2018, **39**, 135-150.

Figures

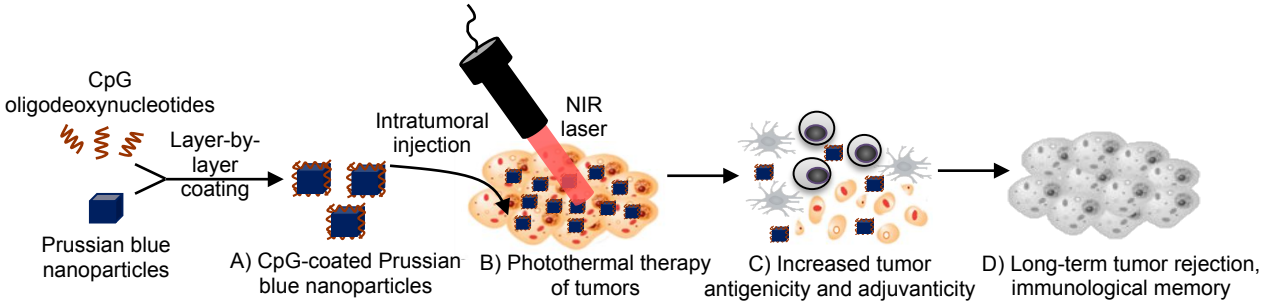

Figure 1. CpG oligodeoxynucleotide-coated Prussian blue nanoparticles (CpG-PBNPs)-mediated nanoimmunotherapy for neuroblastoma. (A) CpG-PBNPs are synthesized via a layer-by-layer coating strategy. (B) The synthesized CpG-PBNPs are intratumorally injected into syngeneic neuroblastoma tumors and activated using a near infrared (NIR) laser effecting photothermal therapy-based ablation of the tumors. (C) The conditions utilized for tumor ablation elicits immunogenic cell death (ICD) in dying tumor cells marked by increased antigenicity and adjuvanticity. (D) The CpG-PBNPs-mediated cell death occurring concurrently with increased antigenicity and adjuvanticity triggers long-term tumor regression and rejection of tumor-rechallenge, suggestive of the generation of immunological memory as a result of the nanoimmunotherapy.

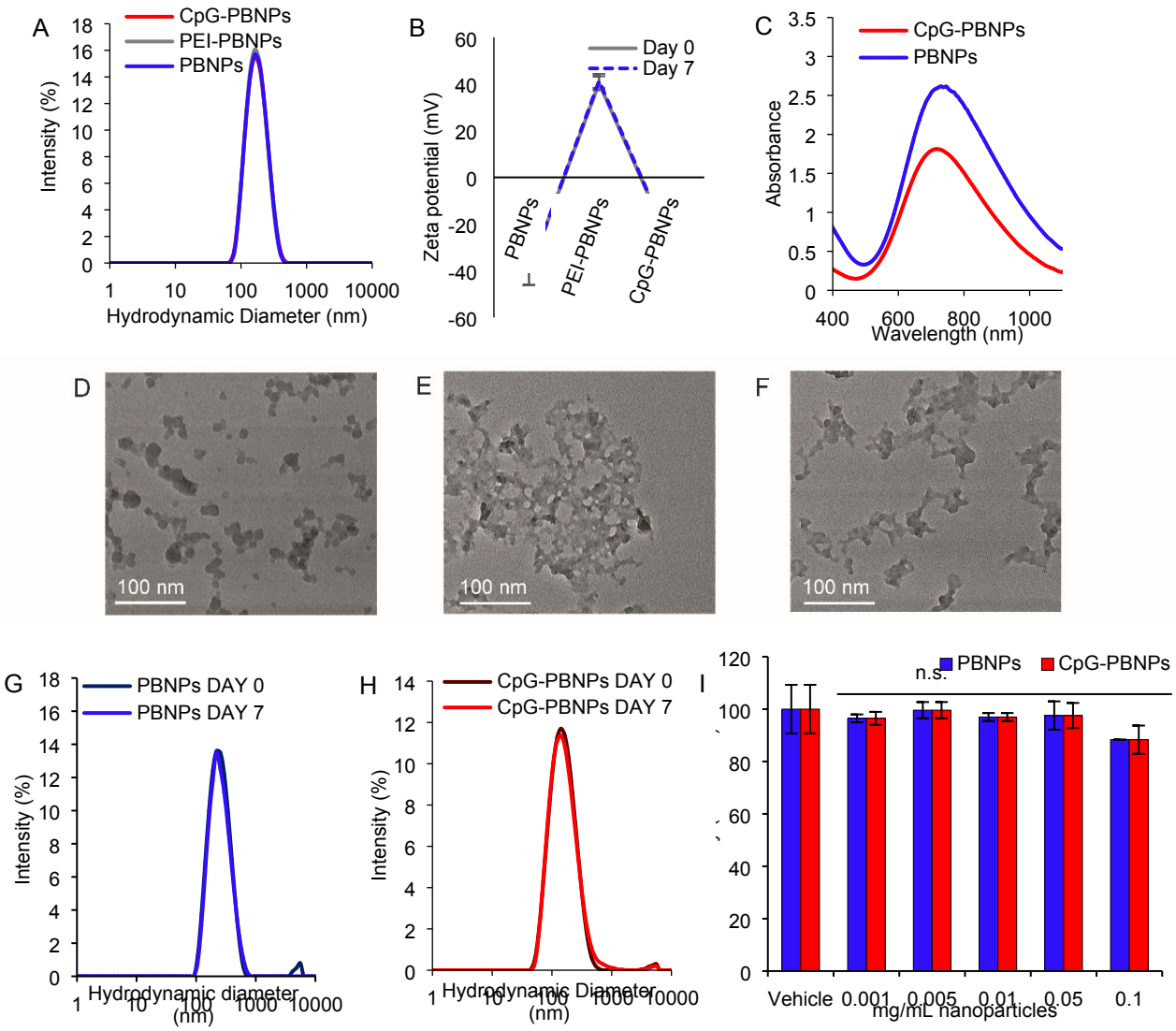

Figure 2. Size distribution, zeta potential, absorbance, multi-day stability, and cytotoxicity of CpG-PBNPs. CpG-PBNPs, as well as the starting (PBNPs) and intermediate nanoparticles (PEI-PBNPs), were characterized using: (A) Dynamic light scattering (DLS), (B) Zeta potential measurements after each step of the synthesis (Days 0 and 7), and (C) Vis-NIR spectra. TEM images of (D) PBNPs, (E) PEI-PBNPs, and (F) CpG-PBNPs. Nanoparticle stability was measured over the course of a week for the (G) PBNPs and (H) CpG-PBNPs using DLS. (I) Cytotoxicity of varying concentrations (0.001 – 0.1 mg/mL) PBNPs and CpG-PBNPs on Neuro2a cells, measured by a cell viability assay (n.s.; no statistical significant difference in viability between both types of nanoparticles and concentrations; $p > 0.05$).

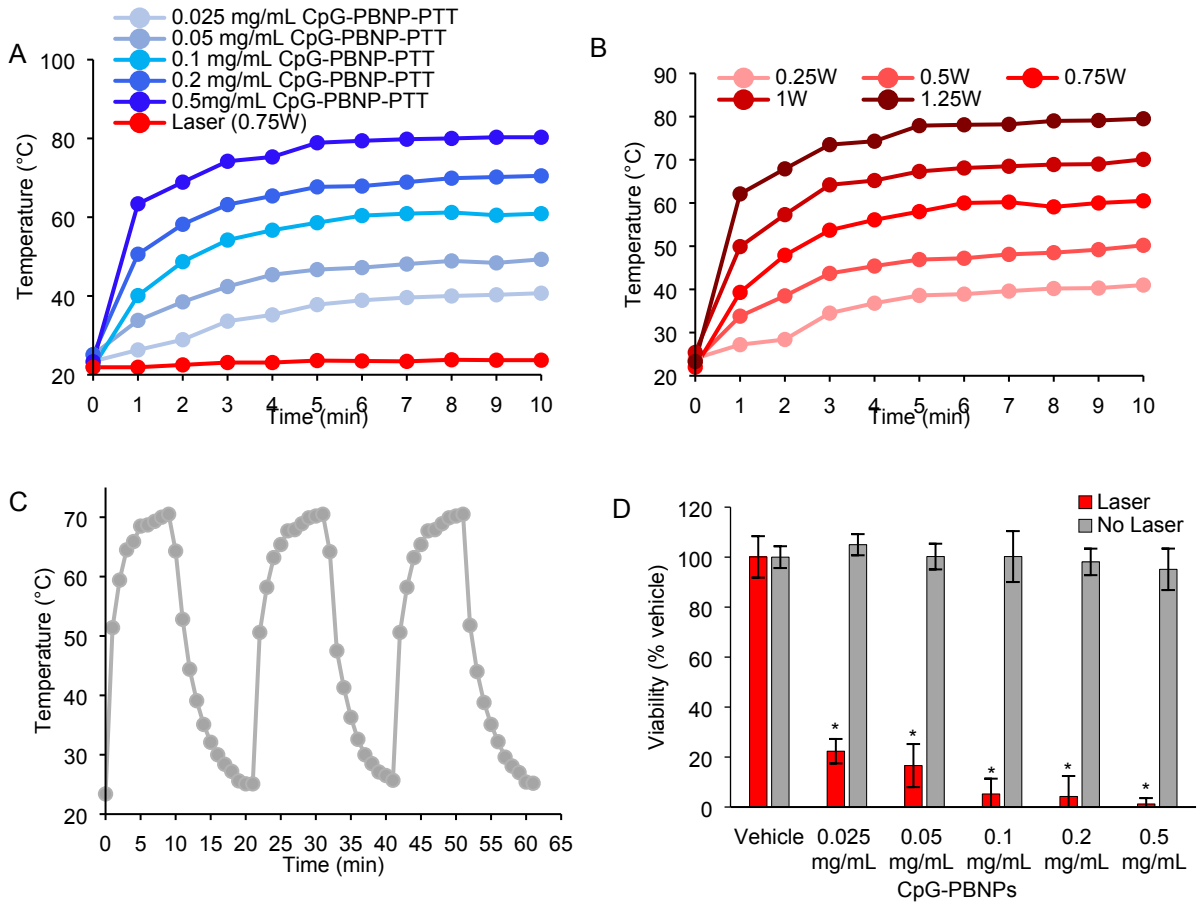

Figure 3. Photothermal properties of CpG-PBNPs. (A) Photothermal heating curves (temperature-time profiles) of varying concentrations (0.025 – 0.5 mg/mL) of CpG-PBNPs irradiated by an 808 nm NIR laser for 10 minutes at a power of 0.75 W (1.875 W/cm^2). (B) Photothermal heating of 1 mg/mL CpG-PBNPs using varying NIR laser powers (0.25 - 1.25 W) for 10 minutes. (C) Temperature profiles during cyclic heating of 1 mg/mL CpG-PBNPs using an 808nm NIR laser at 0.75 W (laser on/off time: 10 minutes each). (D) Neuro2a cell viability *in vitro* post-treatment with vehicle or varying doses of CpG-PBNPs (in the absence or presence of the NIR laser at 0.75 W for 10 minutes), measured 24 h after treatment. (* significant difference, $p < 0.001$ compared with vehicle).

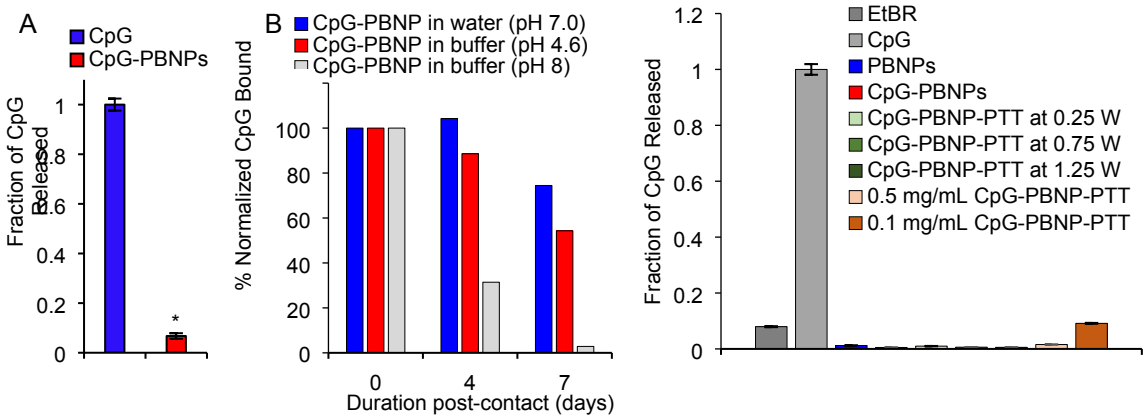

Figure 4. Release of CpG from CpG-PBNPs. (A) Fraction of CpG released from CpG-PBNPs upon addition of ethidium bromide (EtBr) relative to equal concentrations of free CpG added to EtBr (* significant difference, $p < 0.05$). (B) Percent normalized CpG bound in the CpG-PBNPs as a function of time and pH. (C) Fraction of CpG released from CpG-PBNPs after PTT at different laser powers (0.25 – 1.25 W) and different concentrations (0.1 – 0.5 mg/mL). Etbr was added as described above.

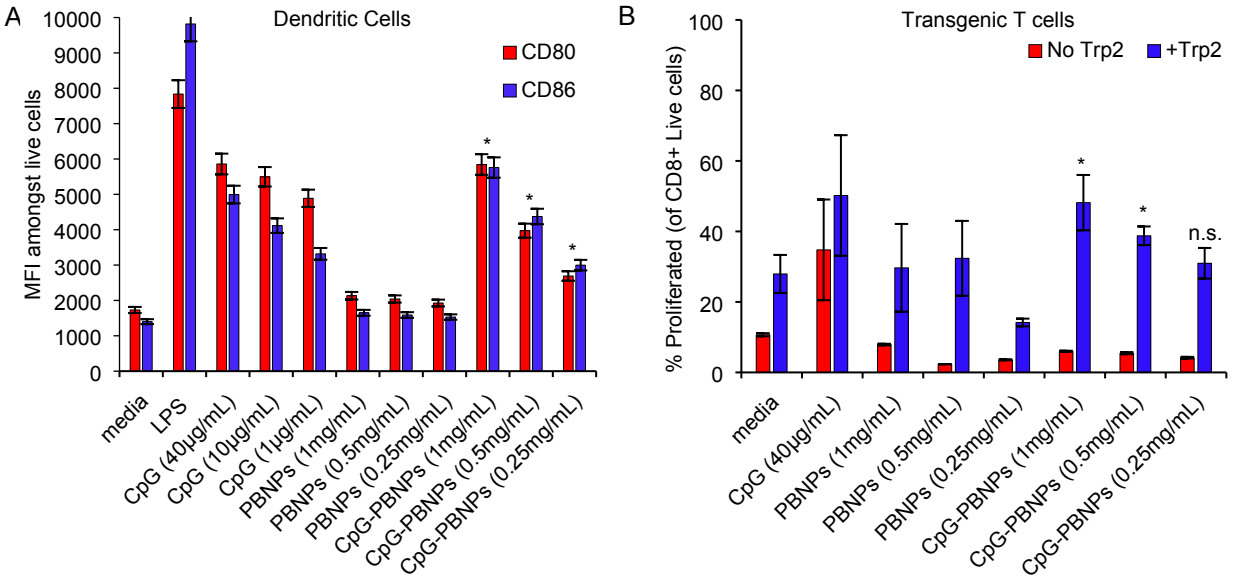

Figure 5. Immunostimulatory properties of CpG-PBNPs. (A) Activation of dendritic cells (DCs) upon co-culture with CpG-PBNPs compared to free CpG, PBNPs, and media controls measured by flow cytometry. CD80 (red) and CD86 (blue) MFI of live CD11c+ positive cells (1 – 0.25 mg/mL). CpG concentrations are as follows: 40 μg/mL, 10 μg/mL, and 1 μg/mL. LPS concentration was 1 μg/mL (* significant difference relative to media-treated DCs for both CD80 and CD86 expression, $p < 0.05$). (B) Percent proliferation of CD8+ T cells co-cultured with DCs activated with CpG-PBNPs and controls (free CpG, PBNPs, and media) (1 – 0.25 mg/mL). Groups were treated with and without the antigen Trp2 (1.25 ng/well). (* significant difference relative to media-treated DCs in the presence of Trp2; $p < 0.05$; n.s., not significant relative to media-treated DCs in the presence of Trp2, $p > 0.05$)

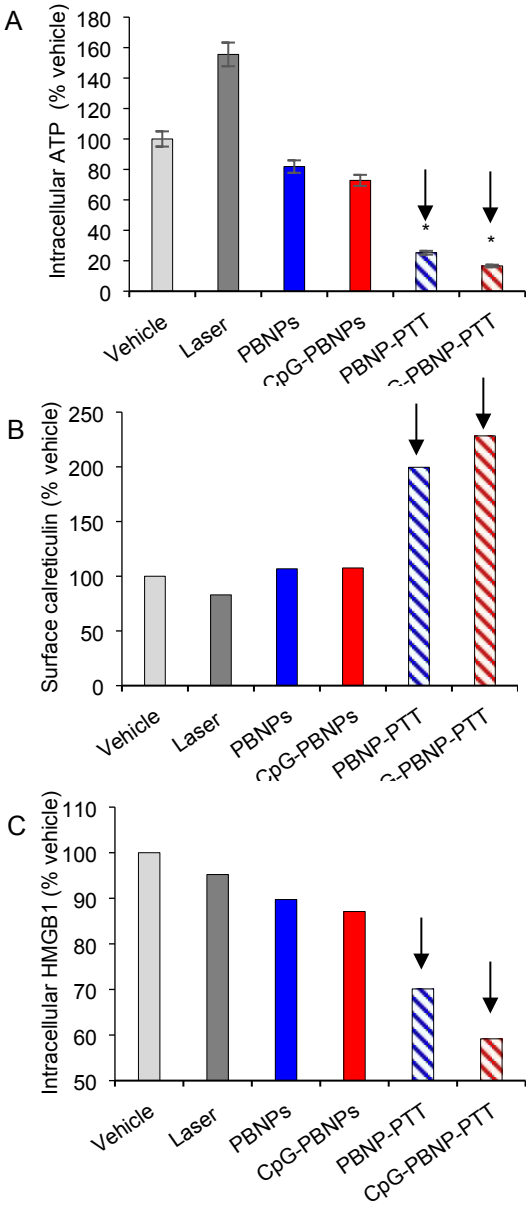

Figure 6. Induction of immunogenic cell death (ICD) by CpG-PBNP-PTT *in vitro*. (A) Intracellular ATP in the various treatment groups (as a % of the vehicle-treated group) (* significant difference relative to vehicle; $p < 0.05$). (B) Surface calreticulin expression in the various treatment groups (as a % of the vehicle-treated group). (C) Intracellular HMGB1 in the various treatment groups (as a % of the vehicle-treated group). All groups had concentrations of nanoparticles at 0.05 mg/mL. PTT groups were treated with a laser power of 0.75W for 10 minutes. Arrows denote the treatment groups where all 3 markers of ICD are expressed/present. Panels B and C were analyzed using flow cytometry and the trends in ICD markers were consistent across at least three separate studies.

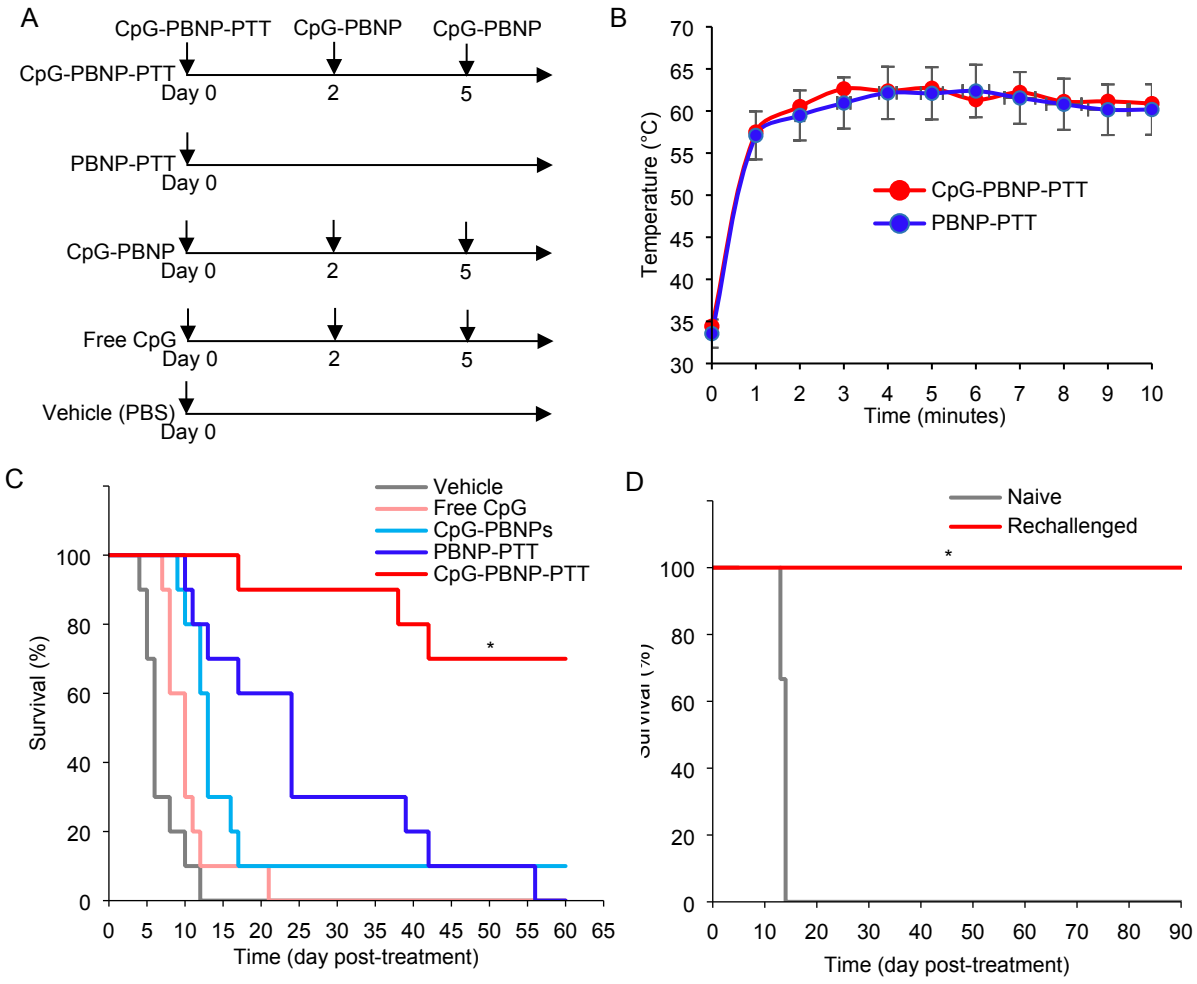

Figure 7. Effect of the CpG-PBNP-based nanoimmunotherapy on tumor regression and long-term survival in the Neuro2a neuroblastoma mouse model. (A) Overview of the treatments. Mice bearing ~5 mm diameter Neuro2a neuroblastoma tumors were treated with CpG-PBNP-PTT and corresponding controls. The PTT-treated groups received 50 μL of 1 mg/mL CpG-PBNPs or PBNPs intratumorally (i.t.), and were irradiated by an 808 nm laser at 0.75 W for 10 minutes. Additionally, the CpG-PBNP-PTT received two boosters with CpG-PBNP on Days 2 and 5. The CpG-PBNP-treated groups received 2 μg of conjugated CpG per dose by i.t. injection (Days 0, 2, and 5). CpG-treated groups received 10 μg of free CpG per dose by i.t. injection (Days 0, 2, and 5). (B) Temperature-time profiles of Neuro2a bearing mice treated intratumorally with 1mg/mL CpG-PBNPs (red) or PBNPs (blue) and irradiated with a NIR laser at 0.75 W for 10 minutes. (C) Kaplan-Meier survival plots of neuroblastoma tumor-bearing mice that were treated with CpG-PBNP-PTT, PBNP-PTT, Free CpG-PBNPs, Free CpG, or vehicle. Mice receiving CpG-PBNP-PTT showed significantly higher long-term survival (>100 days) compared with mice in the other groups (* significant difference compared to all other groups, $p < 0.05$, long-rank test, n=10/group). (D) Long-term surviving mice rechallenged with Neuro2a cells 60-90 days after treatment showed complete tumor rejection (* significant difference compared to naïve mice, $p < 0.05$, n>=7/group).

Table of Contents

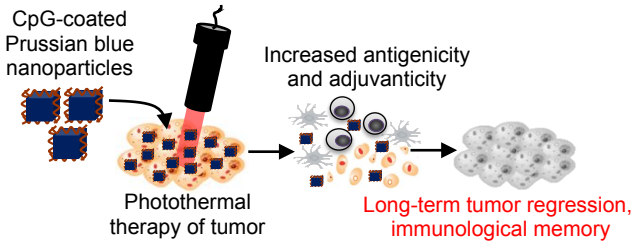

Table of contents entry. Photothermal therapy using CpG oligodeoxynucleotide-coated Prussian blue nanoparticles increases tumor antigenicity and adjuvanticity, eliciting long-term tumor regression and immunological memory